Counterfactual Hypothesis Testing of Tumor Microenvironment Scenarios Through Semantic Image Synthesis

people

1 Abstract

Recent multiplexed cellular protein imaging technologies allow for cells, their spatial organization, and interactions within microenvironments to be characterized at an unprecedented resolution. However, observational data from current imaging alone does not allow users to infer causative relationships and interactions between cells. To address this challenge, we develop a novel generative adversarial network (GAN) architecture, coined Cell-Cell Interaction GAN (CCIGAN), that generates biologically accurate images of cell-cell interactions from semantic cell segmentations. User controllable input variables such as cell types, sizes, and neighborhoods can be adjusted in the cell segmentation to predict spatial, directional, and expression change of cellular proteins in counterfactual cell-cell interaction scenarios. Then to analyze these generated interactions, we develop a data analysis pipeline which allows for rapid hypothesis testing of causative cell-cell interactions. For instance, counterfactual questions such as "how does PD-1 expression on a CD8 T cell change upon exposure to PD-L1 expressing tumor cells?" can be passed into CCIGAN and then tested to quantify the resulting change in cellular protein expression and localization. Scenarios across multiple cell types and protein channels were tested, capturing many fundamental tumor-immune cell interactions. CCIGAN was successful in recapitulating expected patterns in tumor immuno-biology that were not successfully achieved by other state of the art GAN models. CCIGAN further yielded novel biological insights on immune cell-tumor interactions which would be challenging to deduce using in vivo techniques alone.

2 Introduction

Immune - tumor cell interactions within the tumor microenvironment have been implicated in many facets of cancer pathogenesis and treatment (Beatty and Gladney 2015; Swann and Smyth 2007; Verdegaal et al. 2016; Kim et al. 2007; Woo et al. 2012).

These interactions are known to play an important role in tissue biology and impact disease progression, driving oncologic processes such as tumorigenesis and immune escape. Currently, the characterization and analysis of cell-cell interactions remains a challenge. However, recent advances in multiplexed tissue imaging technologies ranging from fluorescence microscopy to ion mass spectrometry have enabled the acquisition of simultaneous cell-cell interactions and their protein localizations at a subcellular resolution, providing unmatched insight into patterns of cellular interactions (Angelo et al. 2014; Keren et al. 2018; Levenson et al. 2015). While these novel technologies are able to image multi-cellular interactions at the single cell level, they present their own set of challenges and have few tools and methods, if any, readily available to interpret and analyze the data at the newly afforded resolution.

Because the interpretation of the multiplexed imaging has the potential to yield novel insights into the nature of the cellular interactions within a specific tissue environment and few methods currently exist to interpret it, there is demand for a tool which can learn from the multiplexed images and generate image-level counterfactual scenarios of cellular interactions within the tumor microenvironment. For example, if a T cell were to migrate into a tumor environment and was surrounded by multiple adjacent tumor cells, how would this change the PD-L1 expression on the T cell? A model that can predict spatial modulations in cell protein localizations, not just their abundance, as a result of changes in neighboring cell environments would provide unique insight into the tissue level biology and pathogenesis driven by individual cell interactions.

How should one integrate effects of nearby cells on protein expression within the cell of interest? Traditional statistics offers potential default strategies, such as binning training examples to quantify effects in particular cases, or regression-type methods to collect information contributed by neighboring cells. While asymptotically workable, when facing finite datasets issues like delineating arbitrary bins, high dimensionality, feature extraction and representation of non-linear effects motivate following generative approaches that have proven successful for other imaging applications, leveraging adversarial neural networks,

We developed a tool, Cell-Cell Interaction Generative Adversarial Network (CCIGAN), which can address both the complexity and limited nature of the multiplexed cell imaging data and allow for the proposition of counterfactual cell interaction scenarios as stated above to better elucidate the interactive processes occurring within a tissue.

The challenge in the development of a tool to analyze multiplexed images is twofold: firstly, addressing with the complexity of the multiplexed images and secondly, addressing with the limited supply of multiplexed data which currently exists. Multiplexed imaging captures many proteins at once, each protein represented as its own channel, resulting in high-dimensional data that is fundamentally different from typical three-channeled red green blue (RGB) images. Thus, applying conventional image analysis methods are not well suited towards

the high dimensionality nature of multiplexed images and would be insufficient in interpreting the multiplexed nature of the data. Additionally, the process of obtaining multiplexed data is a time and labor intensive process, leading to a limited supply of data. Accordingly, searching for specific cell interaction scenarios in exacting cell neighborhoods to be quantified are not readily available or found within the imaged tissues. Ultimately, high dimensionality and lack of data pose unique challenges in image modeling and interpretation.

Existing methods for analyzing cell data can be broadly grouped into two categories, cell classification and cell population analysis, neither of which take advantage of the multiplexed single cell protein expression and resolution to investigate protein localization. Methods for cell classification (Jackson et al. 2020) do not focus on predicting protein expressions and localizations but instead focus on clustering cell-types by protein characteristics. Bayesian model methods for cell-cell interaction analysis (Arnol et al. 2019) do not predict pixel level spatial protein expression but instead predict only a scalar magnitude per protein expression. Some recent GAN-based methods which augment cell imaging data for training purposes (Baniukiewicz et al. 2019) or to synthesize cell images into multiple channels (Osokin et al. 2017) do not study cell cell interactions either. Few conditional cell image synthesis models exist, and they model only a single cell without considering neighboring cells' effects and the multiplexed nature of the data (Johnson et al. 2017; Zhao and Murphy 2007). In contrast, CCIGAN is a generative model that is able to predict multiple channels of protein localization at the pixel level for a cluster of cells to capture both magnitude and spatial information influenced by the cell-cell interactions.

In this investigation, we introduce a framework consisting of a deep generative network and a pipeline for subcellular level image testing and analysis. The first portion, CCIGAN, introduces a novel end-to-end deep architecture capable of conditionally posing cell scenarios not necessarily observed directly in the collected data for rapid counterfactual hypothesis testing. The second portion, the accompanying data analysis pipeline, is used to interpret and explain CCIGAN's outputs at a neighborhood, single cell, and subcellular level in a biologically meaningful manner. Lastly, we include a search algorithm in this framework to automate CCIGAN's output and search for specific cell scenarios that may result in a significant change in protein expression. Our experiments show how the framework provides insight on hypothetical cell interaction events, shedding insight on disease pathogenesis which cannot be feasibly achieved by direct observation of the multiplexed data alone.

3 Results

We first report results that validate the CCGAN methodology from a machine learning, technical perspective. We then walk through a series of positive controls, where CCIGAN rediscovers known biological effects for various cell types (denoted as the cell of interest) due to neighboring cell influences (presented

Technology	Cell of Interest	Marker of interest	Neighboring cell type	Neighbor Protein Channel
MIBI	CD8 T, Endo. CD3 T, Endo., Tumor CD8 T, Tumor Macrophage	PD-1 β-catenin pan-keratin PD-L1	tumor tumor, dendritic CD8 T tumor	PD-L1 dsDNA dsDNA PD-L1
CyCIF	CD8 T CD8 T	PD-1 LAG3	tumor tumor	PD-L1 PD-L1

Table 1: Rediscovery of known cell-cell interactions as positive controls for CCIGAN

in different microenvironments) in the context of simultaneous different protein channels. We present 6 such controls across two different technologies, as detailed in Table 1. We then leverage CCIGAN in discovery mode, to identify new potential such effects.

The CCIGAN Model and Image Analysis Pipeline. We first considered multiplexed images of triple negative breast cancer biopsies (Angelo et al. 2014) and primary lung cancer (Rashid et al. 2019a) were input into CCIGAN. As a deep conditional image synthesis model, CCIGAN takes as input cell segmentation patches (a subsection of the full cell segmentation) (as a cell-typed neighborhood) and outputs a prediction of the proteins expressed on the cells within the segmentation patch (Fig 1). Details on data format and processing

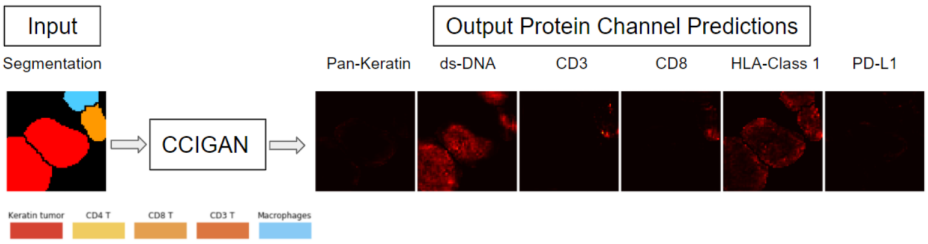

Figure 1: **Input and output of CCIGAN.** Segmentation patch input into CCIGAN and resulting prediction of protein expression in each channel. Output protein expressions are given as 0 to 1 real valued numbers. Labels of the cell type within the segmentation are given on the bottom of the figure.

are given in Online Methods Section 2 (OM.S2). In doing so, CCIGAN learns a many to many mapping between different cell types and different protein markers. Due to its conditional nature, CCIGAN is able to take any segmentation patch as input, such as a patch where a user defines the cells' types, shapes, and neighbors. For our model, changes in protein expression are predicted for a specific cell of interest as a result of adjacent neighboring cells' influences on it. We test counterfactual scenarios by artificially inserting specific cell types

adjacent to our cell of interest within the generated image. This allows us to ask questions such as "what would be the effect on a cell A of interest (type: tumor) of adding cell B (type: CD8 T cell) adjacent to it?" (Fig 2A). The model answers such a question by artificially adding the adjacent cell to the segmentation patch and observing the inferred protein expression change exerted on the cell of interest. Without CCIGAN, isolating and manipulating cells to investigate their independent protein expressions would be problematic because a simple deletion of adjacent cells around the cell of interest would fail to alter the cell of interest's protein localization as it will still assume a neighborhood interaction. An example illustration is given in Supplement S2.3 (S2.3).

Specifically, CCIGAN's convolutional architecture 2B, OM.S1.1) is built on top of spatially adaptive normalization (SPADE) (Park et al. 2019). CCIGAN associates the types, shapes, and relative locations of a cell of interest and its adjacent cells to predict spatial maps of protein expression. The ability of SPADE to modulate the neural network's activations based on the context of adjacent cells allows the network to effectively model the behaviors and interactions for cells of interest. A technical exploration into model interpretability is given in S1.3.

Addressing multiplexed data is critical. This is because of the relative independence of channels dedicated to biological markers, compared to the typical RGB situation. Without addressing this independence, a conventional GAN would equally attend to every location of the current latent representation, even if it is irrelevant to the current protein, making it difficult for a standard RGB multihead decoder to output multiple independent channels. CCIGAN is unique in its ability to tackle such complexity via a novel attention architecture. Since each protein channel is unique, the attention module individually models and conditions the final output of each protein channel on the cell types within the input segmentation patch (Fig 2C). For example, the protein marker pan-keratin (which is typically expressed only in tumor cells), the output of the attention module focuses on generating the spatial protein expression pattern of the tumor cell's pan-keratin while ignoring irrelevant cells. This is achieved through grouped convolutions, learned weights, and Einstein summations (OM.S1.3).

In order to assess the outputs of CCIGAN and extend its utility, we use a series of biologically motivated image analysis techniques and a search algorithm, collectively called the image analysis pipeline. Each of these techniques, cumulative expression, weighted centroid, and directional mass shift, (Fig 3) quantify how one particular cell's protein expression at a pixel wise level reacts to newly introduced adjacent cells.

Model evaluation. CCIGAN is unique among biological tools because current cell image analysis methods either (1) do not perform multichannel or multicellular image synthesis for spatial protein map prediction or (2) consider protein expression counts only and do not predict a protein expression map.

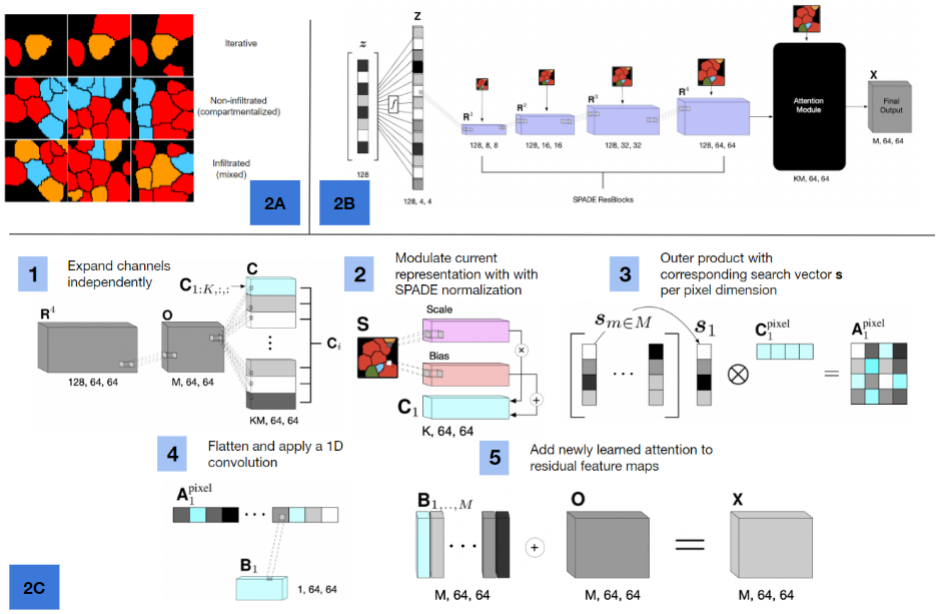

Figure 2: **CCIGAN components. (2A)** Examples of how CCIGAN segmentation maps can be synthetically altered to pose different counterfactual biological scenarios for in silico hypothesis testing. Different colors indicate different cell types. For example, the first row poses the scenario on how adding increased tumor cells (red) around a CD8 T cell may affect the CD8 T cell. The second and third row pose different tumor infiltrated scenarios. **(2B)** An overview of CCIGAN's convolutional architecture. Corresponding equations for the model are given in OM.S1.1. The starting input is a low dimensional noise vector (z) that is convolutionally upsampled and normalized by an input segmentation through a series of spatially adaptive normalizing (SPADE) res-net blocks. Finally the intermediate representation passes through a multiplexed attention module to reason biological relationships. **(2C)** A step by step breakdown of the attention module. Corresponding equations for the attention module are given in OM.S1.2. The module begins by disentangling the fully connected representation into individual channels through grouped convolutions. Afterwards the model uses an outer product attention layer to model relationships and interactions between specific markers and cell types. By using an outer product, the model forces attention at a pairwise pixel level comparison for all combinations of a learned prior vector over markers and different cell types.

To demonstrate CCIGAN's effectiveness, we first benchmark our model (with and without the attention module) against other current state of the art image synthesis techniques through our image analysis pipeline (Fig 3A) to establish biological accuracy and with standard image evaluation criteria on the

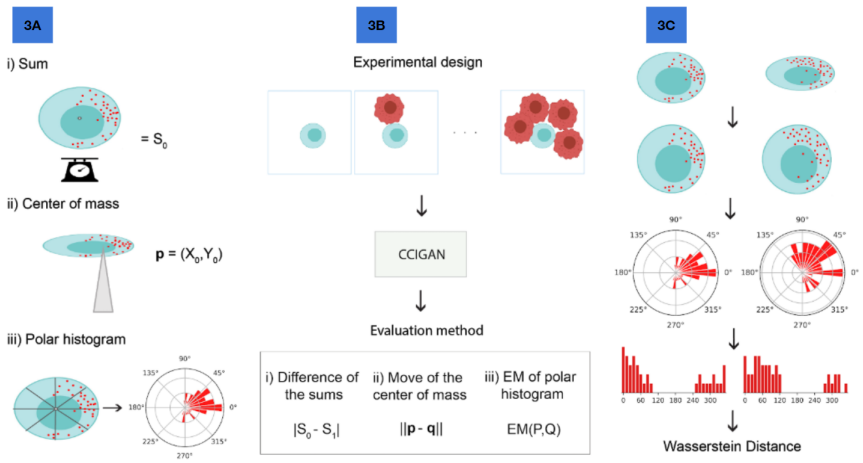

Figure 3: **3: Image Analysis Pipeline.** Blue circles represent a cell, the red dots represent individual protein expressions. To analyze various questions posed by different segmentation arrangements and outputs by CCIGAN, we designed a set of metrics to evaluate the changes in protein expressions of a cell. **(3A)** Evaluation Criteria. They include 3A(i) summing protein total expression of a cell of interest, 3A(ii) computing the center of mass of a protein expression within a cell of interest, and 3A(iii) spatially quantifying the shift in expression of a cell of interest due to changing neighboring cells. **(3B)** Search Algorithm. To further explore potentially unknown interactions, we provide an algorithm to use CCIGAN's predictions and search through different types and arrangements of segmentations with a specified metric (3A). The search algorithm automates CCIGAN's inference to search across a wide range of cell types and parameters. Red circles indicate a cell of a different type. **(3C)** Directional Mass Movement Quantification. In more detail of 3A.iii, to evaluate protein expression spatially and directionally for the cell that is measured, the cell is first warped into a standardized format, interpolating expressions along the way. Second, the cell is binned and a histogram is computed along its polar axis. Finally, center of mass geometries are used as guiding directions to positively or negatively weigh the earth mover's distance in computing the score.

multiplexed ion beam imaging (MIBI) triple negative breast cancer dataset (Angelo et al. 2014). We find that only CCIGAN is able to independently recapitulate established patterns of cell-cell interactions and their biological phenomena while other models fail to learn correct cell-cell interaction associations. We also report CCIGAN's image generation outperforms or matches current methods for standard image evaluation criteria (OM.S3.1).

Applications to Multiplexed Ion Beam Imaging Analysis (MIBI) T cells located within the tumor microenvironment have upregulated expression of PD-1 as a result of the tumor milieu exerting influence on the protein

localization and expression of infiltrating T cells (Ahmadzadeh et al. 2009; Chen et al. 2019; Escors et al. 2018). To corroborate previously established biology on PD-1/PD-L1, we design various tumor and CD8 T cell microenvironments and assess this interaction between adjacent tumor cells and a CD8 T cell of interest. The image analysis pipeline allowed us to ask two questions quantifying this interaction.

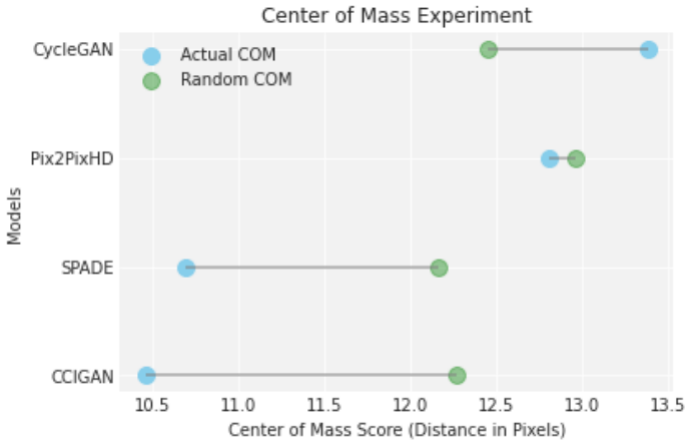

Figure 4: **MIBI PD-1/PD-L1 Center of Mass (COM).** We assess the center of mass (COM) scores where a lower score indicates a more accurate prediction of center of mass. In other words, a lower score indicates that the PD-1 expression on a T cell is more closely localized to where PD-L1 is expressed on neighboring tumor cells. Blue dots indicate the models' scores and green dots indicate the control which is a randomly selected point representing a randomly selected PD-1 center of mass on a T cell. Larger differences between the models' scores (blue) and the control experiment (green) indicate that the model is more successful in capturing the true response of PD-1in a real scenario.

First, we examined how PD-L1 expression in adjacent tumor cells affects PD-1 expression and localization in a CD8 T cell of interest (Fig 3A.ii). The center of mass of the CD8 T cell's PD-1 expression was used as a proxy for its localization, and adjacent tumor cells' PD-L1 protein expression center of mass was used as a proxy for cell contact. The score itself represents the distance in pixels between the PD-1 and PD-L1 centers of mass (OM Eq. 13). We run this in silico experiment (Fig 4, OM.S3.2, S3.1), and demonstrate CCIGAN's ability to provide the best expected predictor of PD-L1 center of mass expression. In comparison, other methods such as Pix2PixHD (Wang et al. 2018) and CycleGAN (Zhu et al. 2017) do not yield any meaningful biological insight and CCIGAN outperforms SPADE (Park et al. 2019) in achieving the most accurate PD-1 center of mass prediction.

Secondly, we focused on directional PD-1 expression in a CD8 T cell of

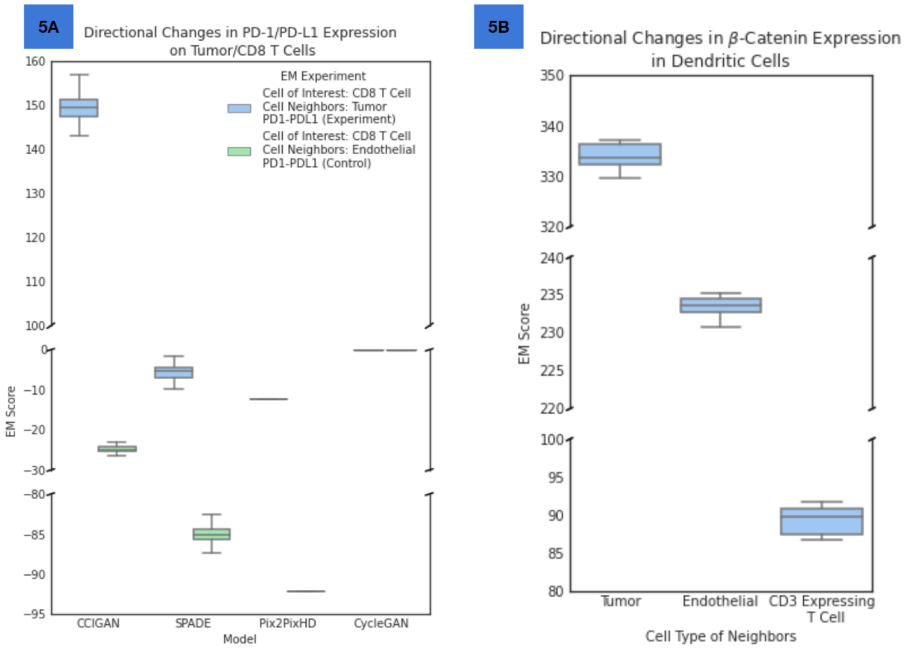

Figure 5: **MIBI Earth Mover's Distance (EM) Experiments. (5A)** In a more granular experiment, spatial and direction image aspects were considered. PD-1 expression shifts due to PD-L1 expressing cell neighbors were measured in a CD8 T cell (cell of interest) by the EM Score (OM.eq.15). A stronger magnitude EM score indicates a stronger cell-cell interaction. A positive value indicates the direction of protein localization moving towards additional cell neighbors and a negative value otherwise. CCIGAN's output supports a significant cell-cell interaction between tumor PD-L1 and CD8 T cell PD-1, inline with clinical studies, but not between the endothelial control cells and CD8. Furthermore, the endothelial control serves as a baseline comparison to gauge the magnitude of tumor PD-L1 and CD8 T cell PD-1 interactions. Other models predict entirely erroneous changes in expression for these interactions. **(5B)** Spatial and directional change in β-catenin expressed in dendritic cells (DCs) as a result of variations in its cell neighbors. A larger positive EM score denotes a stronger cell-cell interaction where the center of mass of the DC's β-catenin shifted towards the neighboring cell contact. CCIGAN output suggests a strong impact of tumor-DC cell interaction on Wnt activation in the DC cell. This strength of interaction is suggestive of the tumor's immunosuppressive effects on the DC.

interest. We sought to quantify the influence of PD-L1 expression in neighboring tumor cells on such directional expression (Fig 3A.iii, Fig 3C, OM.S3.3). The hypothesis in this in silico experiment is increased directional PD-1 expression

in the cell of interest as a result of the iterative introduction of adjacent PD-L1 expressing tumor cells (Fig 5A). As a control, a PD-1 expressing T cell was surrounded with endothelial cells. Our initial hypothesis was confirmed in CCIGAN's predictions, where the presence of a PD-L1 expressing tumor cell induced an increase in PD-1 expression in the CD8 T cell and a shift towards the PD-L1 center of mass on surrounding tumor cells. This was not observed in the control experiment. Increasing endothelial cell presence did not yield a significant directional effect on the T cell's PD-1 expression. Furthermore, a significantly smaller spatial PD-1 expression increase in the T cell was observed. PD-L1 is naturally found on a variety of endothelial cell types and serves as an immunomodulatory checkpoint that plays an important role in protecting normal cells from T cell driven autoimmune reactions (Eppihimer et al. 2002; Rodig et al. 2003). The model's assessment of CD8 T cell - endothelial cell interaction resulting in a small increase in T cell PD-1 expression is therefore biologically expected. The magnitude and directional effect which the tumor's PD-L1 had on T cell PD-1 expression highlights the greater degree to which this immunomodulatory checkpoint is exploited by malignant cells to escape immune detection.

While both tumor and endothelial cells express PD-L1, the tumor microenvironment exercises more complex suppressive effects on CD8 T cells, which are more likely to modulate T cell activation than endothelial cells. Off the shelf methods SPADE, Pix2PixHD, and CycleGAN fail to capture this interaction. We then applied our directional mass movement experiments towards the Wnt cellular signalling pathway in dendritic cells (DCs). The downstream effects of the Wnt pathway results in an increase in the cellular β-catenin. We were interested in exploring the directional expression of β-catenin induced by DC (cell of interest) interactions with varying adjacent cell types (neighboring cells) (Fig 5B). As a proxy for cell proximity, we used dsDNA to indicate cell relation to the DC beta catenin expression to measure mass movement. Wnt induction on DCs by tumor cells plays an important role in the modulation of antitumor immunity by suppressing DC activation (Swafford and Manicassamy 2015) and we expected that increasing tumor cell presence adjacent to DCs would result in an immunosuppressive cascade in the DC that would be identifiable by a directional increase in in the DC's β-catenin. The results of our experiments demonstrated that tumor cells adjacent to DC cells resulted in an EM score of 333.9 (denoting a greater directional magnitude of cell-cell interaction), larger than which was seen in situations where DC cells were adjacent to endothelial cells (EM score: 233.6) and CD3 expressing T cells (EM Score: 89.3). These findings confirm our hypothesis that (1) CCIGAN is capable of detecting directionally-dependent patterns associated with the activation of the Wnt pathway and (2) that CCIGAN captures the biologically expected tumor-mediated activation of the Wnt pathway on DCs.

We further analyzed another interaction (Fig 6, OM.S3.4, S3.4), assessing the effect of neighboring immune cells on status markers within a tumor cell of interest. Keratins are a class of intracellular proteins that play an important

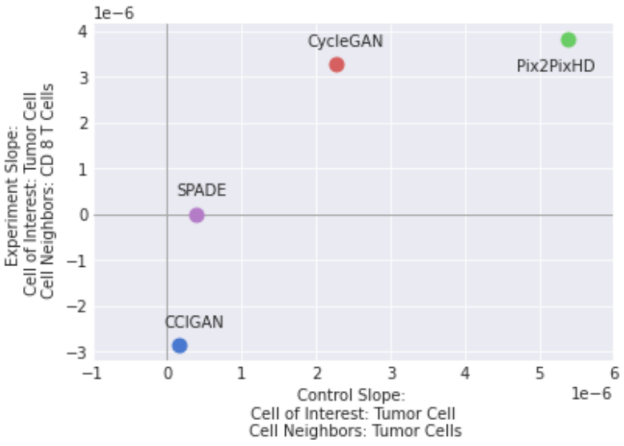

Figure 6: **Regression slopes Experiment (MIBI)** When comparing CD8 T cell influences on pan keratin pixel level expressions, we observe that as a tumor cell of interest is increasingly surrounded by CD8 T cells it experiences a decrease in total pan-keratin expression. Conversely, in a control experiment where a tumor cell of interest is surrounded by other tumor cells, there is no significant trend in pan keratin. The slope values in the graph represent rates of change in the pan-keratin expression as a function of additional CD8 T cell neighbors. CCIGAN was the only method which captured a drop in tumor pan-keratin expression with CD8 T cell neighbors but no change under the control conditions.

role in ensuring cell structure (Azumi and Battifora 1987). Furthermore, when CD8 T cells mediate tumor killing, they release granzymes or induce extrinsic apoptosis which results in the release of enzymes responsible for cleaving the tumor cell's pan-keratin, disrupting the tumor cell structure (Martínez-Lostao et al. 2015) (Oshima 2002) (Badock et al. 2001) (Ku et al. 2016). We explored how a drop in pan-keratin levels in the tumor cell of interest could be used as a proxy marker for the likelihood of tumor cell death in the presence of varying adjacent CD8 T cells. Since the input cell segmentation indicates the existence of a tumor cell, cell death cannot be represented by cell destruction and can only be inferred via change in pan keratin expression.

We observed that the introduction of adjacent CD8 T cells to a tumor cell decreased the pan-keratin expression in the tumor cell. This effect became more dramatic as the number of surrounding CD8 T cells increased. As a control, when the tumor cell of interest was introduced to adjacent tumor cells instead of CD8 T cells, no change was noted in the tumor cell's pan-keratin for CCIGAN. Other methods reported contrasting results where a significant change in the tumor cell pan-keratin expression was incorrectly reported under the control conditions. These results indicate that an increasing T cell presence mitigates

a decrease in the predicted pan-keratin expression in the tumor cell, suggesting a decreased probability in tumor cell existence.

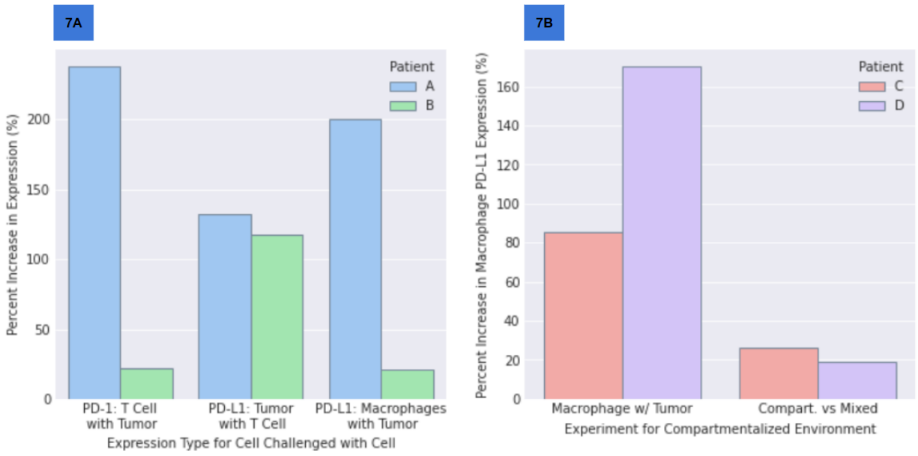

Figure 7: **Comparmentalized and Non-compartmentalized Microenvironment Experiments (MIBI) (7A)** Graph demonstrating the percentage increase in the PD-1 or PD-L1 expression induced by cell-cell interactions in individual patient data. In both patients, T cells with introduced tumor cell neighbors noted an increased PD-1 expression. Similarly, tumor cells with introduced T cell neighbors and macrophages with introduced tumor cell neighbors both resulted in increased PD-L1 expression for the cell of interest, as expected from the literature. **(7B)** An increase in macrophage PD-L1 expression upon introduction of a tumor cell neighbor is reported within a compartmentalized tumor environment. There is an overall greater PD-L1 expression by macrophages in compartmentalized environments than mixed ones, a finding which recapitulates previous literature.

In another replication study (Fig 7, S3.5), we corroborate and further quantify an analysis done on the variability of PD-L1 expression in macrophage and tumor cells across TNBC patient groups within the MIBI dataset. The outcomes of this experiment corroborate the biological findings reported on the same data in Keren et al. (2018) (Keren et al. 2018). Here, we demonstrate that when the model is trained using individual patient samples, as opposed to multi-sample datasets, it continues to recapitulate biologically validated patterns of tumor-immune cell interactions reported in the literature.

Lastly, we use our search algorithm to extend to other cell-cell interactions (Fig 8). While most changes in protein expressions are plausible and/or significant, there are some erroneous correlations (a CD 8 T cell expressing PD-L1 while in close contact to tumor cells) that are attributed to poor segmentations, imaging faults, and other noisy effects. In other experiments, we not only

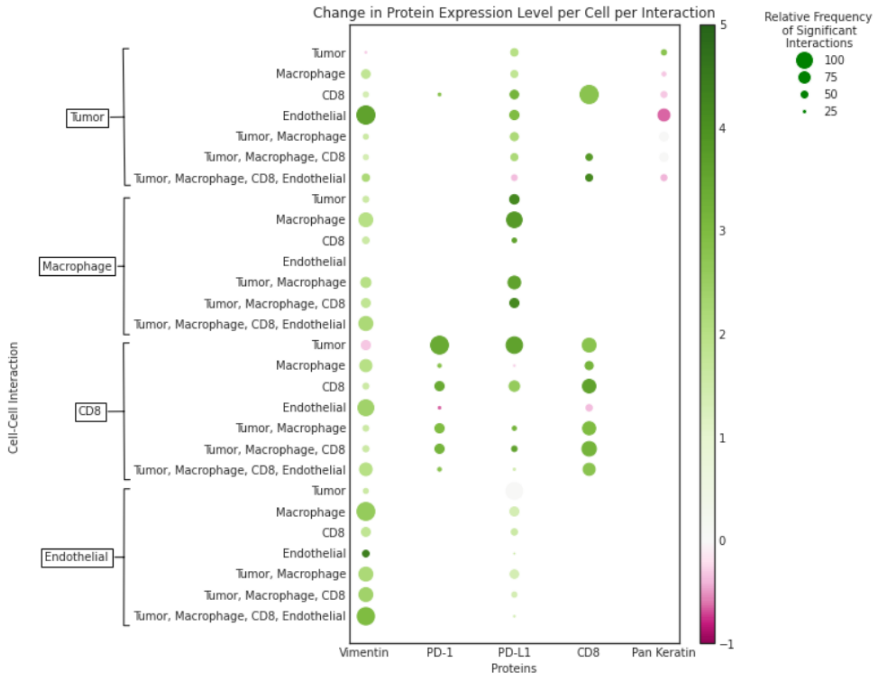

Figure 8: **Search Algorithm Results - Specific cell-cell interactions and the associated magnitude of change in protein expression.** The cell types in boxes on the y-axis are the cell of interest in the experiment. The cell names adjacent to them represent their neighbors. The diameter of the circle marker represents the relative frequency by which this specific cell - cell interaction induced a non-trivial change in the expression of a given protein. The hue of each circle illustrates the magnitude of that change in expression level. For example, we see that when a CD8 T Cell (boxed, y-axis) has a tumor cell neighbor (y-axis) there are significant interactions which induce a change in the CD8 T cell's PD-1 expression. From these interactions there was on average an order of 3 increase in PD-1 expression.

confirm our previous findings but also posit further interactions of biological significance for later exploration. A further discussion and investigation to these cell-cell interactions, and in particular, vimentin, are given in S4.2.

Vimentin plays an important role in tumorigenesis both as a structural protein and in cellular signalling. Numerous studies have noted vimentin's regulatory importance in a variety of cell signalling pathways which promote tumor survival and resistance to cellular stress (Arun and Shulin 2011) (Kidd et al. 2014). CCIGAN experiments wherein a tumor cell of interest was surrounded by increasing numbers of CD8 T cells caused up to a 91.6% increase in the total

tumor vimentin expression (S4.2.1). Increasing CD8 T cell presence around a tumor cell is likely to be associated with increasing amounts of pro-apoptotic signalling on the tumor cell, causing a large degree of cellular stress. Thus the increase in the tumor's vimentin would be a biologically expected outcome given the protein's role in promoting cellular survival pathways.

Applications to Tissue Cyclic Immunofluorescence (t-CyCIF) t-CyCIF data is obtained through a novel iterative immunofluorescence staining procedure that works with existing fluorescence microscopes (Lin et al. 2018). By applying CCIGAN to a t-CyCIF primary lung cancer image dataset (Rashid et al. 2019b), we demonstrate CCIGAN's ability to generalize across datasets and learn microenvironment-specific cell-cell interactions.

Utilizing a lung cancer patient's t-CyCIF tissue sample that demonstrated progressive tumor cell growth, we split the image data according to three different stages of immune cell tumor-infiltration – poorly-infiltrated (T_1, semi-infiltrated (T_2), and heavily-infiltrated (T_3) (S2.2.2). We denote each stage as a separate microenvironment and apply CCIGAN by training a model per microenvironment to summarize its cell-cell interactions. Training microenvironment-specific models also allows for differential analysis of protein-level interactions.

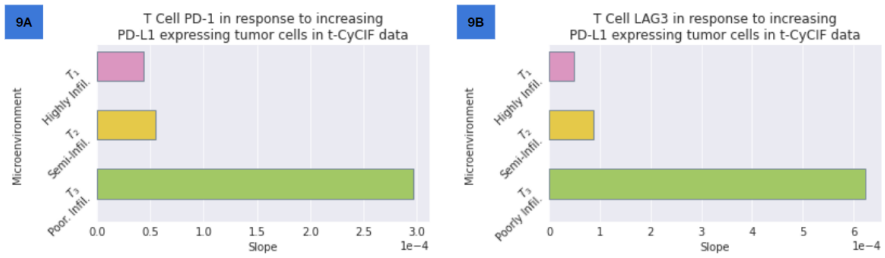

Figure 9: **CyCIF Trends**. **(9A)** PD-1 expression on CD8 T cells as a function of number of PD-L1 expressing tumor cell neighbors and type of tumor environment. In an infiltrated environment (high proportion of lymphocyte presence within the tumor microenvironment, indicative of a strong inflammatory anti-tumor immune response) there is reduced PD-1 expression on infiltrating T cells indicating a more robust anti-tumor immune response. **(9B)** LAG3 expression on CD8 T cells as a function of PD-L1 expressing tumor cell neighbors and type of tumor environment. In an infiltrated environment there is a decrease in T cell LAG3 expression indicating reduced T cell exhaustion in situations where there is a robust anti-tumor immune response.

Similar to the CD8/pan keratin trend experiment (Fig 9A, S3.6), we examine the correlation between PD-1 and PD-L1 in tumor and T-cell patches in each microenvironment-specific model. In the non-infiltrated microenvironment model, we observe a higher trend in T-cell PD-1 expression as a function of tumor area than in the other two microenvironments, semi-infiltrated and

heavily-infiltrated. These findings can be biologically justified by the fact that a poorly lymphocyte-infiltrated tumor has succeeded in suppressing anti-tumor inflammatory immune responses and thus an increase in PD-1 expression on the T cell would be expected, denoting increased immunosuppression by the tumor.

The semi-infiltrated microenvironment also shows a higher trend than the heavily-infiltrated microenvironment. In other words, a tumor-immune microenvironment that is progressively more immune infiltrated resulted in a steady decrease in total PD-1 expression on CD8 T cells, denoting a greater inflammatory immune response to the tumor microenvironment. This observation confirms our hypothesis that CCIGAN learns the appropriate cell-cell interactions found in microenvironments with higher rates of tumor-infiltration.

In a similar fashion (Fig 3G, S3.6), we examined the association between LAG3 (Long et al. 2018) (Andrews et al. 2017) expression on T cells (a marker of T cell exhaustion) and PD-L1 expression on neighboring tumor cells. The experimental scenario involved a CD8 T cell cell of interest that was surrounded by an increasing number of PD-L1 expressing tumor cell neighbors. An increase in T cell expression of LAG3 with increasing PD-L1 expressing tumor neighbors was found in all three scenarios (non-infiltrated tumor, semi-infiltrated tumor, and infiltrated tumor). Furthermore, T cell LAG3 expression decreased in progressively more immune infiltrated tumor scenarios. These results correlate with the expected biological outcomes. Firstly, that increased tumor PD-L1 expression would suppress T cell function and induce T cell exhaustion and secondly, that T cells within more infiltrated tumor environments (associated with greater anti-tumor immune responses) had reduced LAG3 expression indicating reduced T cell exhaustion.

The findings from the t-CyCIF experiments highlight the utility of CCIGAN in reliably reproducing biologically expected patterns of immune cell - tumor cell interaction from even limited patient tumor samples. Furthermore, CCIGAN demonstrates added value in its ability to provide robust quantifications of protein expression changes as a result of cell-cell interactions.

4 Discussion

While multiplexed imaging technologies continue to rapidly increase in resolution and availability, tools to analyze and interpret their outputs remain either nonexistent or primitive. Specifically, current methods either do not investigate protein localization in cell-cell interactions or do not account for spatial information, cell neighborhood influences, and the multiplexed nature of the data for analysis. Furthermore, they remain limited by the scarcity of data due to the time and labor intensive process. To address these limitations we introduced the idea of applying image synthesis in the form of a novel generative architecture, CCIGAN, and developed a computational image analysis pipeline to interpret

CCIGAN's outputs. By simultaneously and generatively associating cell shapes, type, and sizes to their protein expression patterns, CCIGAN allows users to specify these parameters in a test environment to pose counterfactual cell-cell scenarios and observe their resulting protein expressions. Subsequently, using the provided image analysis pipeline, users are able to interpret and quantify the protein expressions at the subcellular level as a function of their defined variables.

The ability for CCIGAN to generate subcellular protein predictions represents a step forward in the ability to understand cellular relationships within a microenvironment. Rather than assessing in vivo incidence of cell interaction phenomena, CCIGAN allows for hypothetical biological situations to be generated and analyzed. In other words, any individual cellular responses to a neighborhood of cells of any identity can be assessed without having to seek this specific occurrence within the available biological tissue sample, addressing the issue of limited multiplexed data.

To demonstrate CCIGAN's accuracy and ability to probe oncological elements, we demonstrated not only its ability to outperform state of the art image synthesis methods but also its ability to capture, recapitulate, and quantify previously clinically established cell-cell interactions. Additionally, we identify a host of cell-cell interactions in the context of their protein expressions that lay the groundwork for exploring and guiding further potentially interesting cellular interactions. Lastly, we establish CCIGAN's flexibility across technologies through experiments on mass-spectronomy and immunofluorescence based images.

Despite the advancements in imaging technology, immediately available data makes investigating further cell-cell interactions difficult as the provided protein channels are typically used for cell typing instead of studying cell localization. However, as these technologies become more pervasive and widely available, more protein markers for protein localization will also become available, further indicating the need for CCIGAN. While we have presented a promising rapid hypothesis testing tool for in silico predictions of various cell-cell interactions, further validation through in CCIGAN guided in vivo experiments corroborating CCIGAN's quantified predictions would provide additional confidence. Current limitations in the model are neither in the architectural nor computational capacity, but rather the input data's noisy cell segmentations and type classifications. While the model does well to learn and associate clearly delineated trends and could potentially correct for erroneous classifications, exceedingly rare cell-cell protein interactions may be interpreted as noise or with low confidence. Nonetheless, given the strong corroboration with previous clinically established biology, the utility in giving user freedom and control to posit new interactions to guide further experiments, we expect this work to be useful in the multiplexed imaging domain.

References

M. Ahmadzadeh, L. A. Johnson, B. Heemskerk, J. R. Wunderlich, M. E. Dudley, D. E. White, and S. A. Rosenberg. Tumor antigen–specific CD8 T cells infiltrating the tumor express high levels of PD-1 and are functionally impaired. *Blood*, 114(8):1537–1544, 08 2009. ISSN 0006-4971. doi: 10.1182/blood-2008-12-195792. URL https://doi.org/10.1182/blood-2008-12-195792.

L. P. Andrews, A. E. Marciscano, C. G. Drake, and D. A. Vignali. Lag 3 (cd 223) as a cancer immunotherapy target. *Immunological reviews*, 276(1):80–96, 2017.

M. Angelo, S. C. Bendall, R. Finck, M. B. Hale, C. Hitzman, A. D. Borowsky, R. M. Levenson, J. B. Lowe, S. D. Liu, S. Zhao, Y. Natkunam, and G. P. Nolan. Multiplexed ion beam imaging of human breast tumors. *Nature medicine*, 20(4):436–442, 04 2014. doi: 10.1038/nm.3488. URL https://pubmed.ncbi.nlm.nih.gov/24584119.

D. Arnol, D. Schapiro, B. Bodenmiller, J. Saez-Rodriguez, and O. Stegle. Modeling cell-cell interactions from spatial molecular data with spatial variance component analysis. *Cell Reports*, 29(1):202 – 211.e6, 2019. ISSN 2211-1247. doi: https://doi.org/10.1016/j.celrep.2019.08.077. URL http://www.sciencedirect.com/science/article/pii/S2211124719311325.

S. Arun and L. Shulin. Vimentin as a potential molecular target in cancer therapy or vimentin, an overview and its potential as a molecular target for cancer therapy. *Cell Mol Life Sci*, 68(18):3033–3046, 2011.

N. Azumi and H. Battifora. The distribution of vimentin and keratin in epithelial and nonepithelial neoplasms: a comprehensive immunohistochemical formalin-and alcohol-fixed tumors. *American journal of clinical pathology*, 88 (3):286–296, 1987.

V. Badock, U. Steinhusen, K. Bommert, B. Wittmann-Liebold, and A. Otto. Apoptosis-induced cleavage of keratin 15 and keratin 17 in a human breast epithelial cell line. *Cell Death & Differentiation*, 8(3):308–315, 2001.

P. Baniukiewicz, E. J. Lutton, S. Collier, and T. Bretschneider. Generative adversarial networks for augmenting training data of microscopic cell images. *Frontiers in Computer Science*, 1:10, 2019. ISSN 2624-9898. doi: 10.3389/fcomp.2019.00010. URL https://www.frontiersin.org/article/10.3389/fcomp.2019.00010.

G. L. Beatty and W. L. Gladney. Immune escape mechanisms as a guide for cancer immunotherapy. *Clinical Cancer Research*, 21(4):687–692, 2015. ISSN 1078-0432. doi: 10.1158/1078-0432.CCR-14-1860. URL https://clincancerres.aacrjournals.org/content/21/4/687.

S. Chen, G. A. Crabill, T. S. Pritchard, T. L. McMiller, P. Wei, D. M. Pardoll, F. Pan, and S. L. Topalian. Mechanisms regulating pd-l1 expression on tumor and immune cells. *Journal for ImmunoTherapy of Cancer*, 7(1):305, 2019.

M. J. Eppihimer, J. Gunn, G. J. Freeman, E. A. Greenfield, T. Chernova, J. Erickson, and J. P. Leonard. Expression and regulation of the pd-l1 immunoinhibitory molecule on microvascular endothelial cells. *Microcirculation (New York, N.Y. : 1994)*, 9(2):133–145, 04 2002.

D. Escors, M. Gato-Cañas, M. Zuazo, H. Arasanz, M. J. García-Granda, R. Vera, and G. Kochan. The intracellular signalosome of pd-l1 in cancer cells. *Signal transduction and targeted therapy*, 3:26–26, 09 2018.

H. W. Jackson, J. R. Fischer, V. R. T. Zanotelli, H. R. Ali, R. Mechera, S. D. Soysal, H. Moch, S. Muenst, Z. Varga, W. P. Weber, and B. Bodenmiller. The single-cell pathology landscape of breast cancer. *Nature*, 578(7796):615–620, 2020. doi: 10.1038/s41586-019-1876-x. URL `https://doi.org/10.1038/s41586-019-1876-x`.

G. R. Johnson, R. M. Donovan-Maiye, and M. M. Maleckar. Generative modeling with conditional autoencoders: Building an integrated cell, 2017.

L. Keren, M. Bossé, D. Marquez, R. Angoshtari, S. Jain, S. Varma, S.-R. Yang, A. Kurian, D. Valen, R. West, S. Bendall, and M. Angelo. A structured tumor-immune microenvironment in triple negative breast cancer revealed by multiplexed ion beam imaging. *Cell*, 174:1373–1387.e19, 09 2018. doi: 10.1016/j.cell.2018.08.039.

M. E. Kidd, D. K. Shumaker, and K. M. Ridge. The role of vimentin intermediate filaments in the progression of lung cancer. *American journal of respiratory cell and molecular biology*, 50(1):1–6, 2014.

R. Kim, M. Emi, and K. Tanabe. Cancer immunoediting from immune surveillance to immune escape. *Immunology*, 121(1): 1–14, 05 2007. doi: 10.1111/j.1365-2567.2007.02587.x. URL `https://pubmed.ncbi.nlm.nih.gov/17386080`.

N.-O. Ku, P. Strnad, H. Bantel, and M. B. Omary. Keratins: Biomarkers and modulators of apoptotic and necrotic cell death in the liver. *Hepatology*, 64 (3):966–976, 2016.

R. M. Levenson, A. D. Borowsky, and M. Angelo. Immunohistochemistry and mass spectrometry for highly multiplexed cellular molecular imaging. *Laboratory Investigation*, 95(4):397–405, 2015. doi: 10.1038/labinvest.2015.2. URL `https://doi.org/10.1038/labinvest.2015.2`.

J.-R. Lin, B. Izar, S. Wang, C. Yapp, S. Mei, P. M. Shah, S. Santagata, and P. K. Sorger. Highly multiplexed immunofluorescence imaging of human tissues and tumors using t-cycif and conventional optical microscopes. *Elife*, 7, 2018.

L. Long, X. Zhang, F. Chen, Q. Pan, P. Phiphatwatchara, Y. Zeng, and H. Chen. The promising immune checkpoint lag-3: from tumor microenvironment to cancer immunotherapy. *Genes & cancer*, 9(5-6):176, 2018.

L. Martínez-Lostao, A. Anel, and J. Pardo. How do cytotoxic lymphocytes kill cancer cells?, 2015.

R. Oshima. Apoptosis and keratin intermediate filaments. *Cell Death & Differentiation*, 9(5):486–492, 2002.

A. Osokin, A. Chessel, R. E. Carazo-Salas, and F. Vaggi. Gans for biological image synthesis. *CoRR*, abs/1708.04692, 2017. URL `http://arxiv.org/abs/1708.04692`.

T. Park, M. Liu, T. Wang, and J. Zhu. Semantic image synthesis with spatially-adaptive normalization. *CoRR*, abs/1903.07291, 2019. URL `http://arxiv.org/abs/1903.07291`.

R. Rashid, G. Gaglia, Y.-A. Chen, J.-R. Lin, Z. Du, Z. Maliga, D. Schapiro, C. Yapp, J. Muhlich, A. Sokolov, P. Sorger, and S. Santagata. Highly multiplexed immunofluorescence images and single-cell data of immune markers in tonsil and lung cancer. *Scientific Data*, 6(1):323, 2019a. doi: 10.1038/s41597-019-0332-y. URL `https://doi.org/10.1038/s41597-019-0332-y`.

R. Rashid, G. Gaglia, Y.-A. Chen, J.-R. Lin, Z. Du, Z. Maliga, D. Schapiro, C. Yapp, J. Muhlich, A. Sokolov, et al. Highly multiplexed immunofluorescence images and single-cell data of immune markers in tonsil and lung cancer. *Scientific Data*, 6(1):1–10, 2019b.

N. Rodig, T. Ryan, J. Allen, H. Pang, N. Grabie, T. Chernova, E. Greenfield, S. C. Liang, A. Sharpe, A. Lichtman, and G. Freeman. Endothelial expression of pd-l1 and pd-l2 down-regulates cd8+ t cell activation and cytolysis. *European Journal of Immunology*, 33(11):3117–3126, 2003. doi: 10.1002/eji.200324270. URL `https://onlinelibrary.wiley.com/doi/abs/10.1002/eji.200324270`.

D. Swafford and S. Manicassamy. Wnt signaling in dendritic cells: its role in regulation of immunity and tolerance. *Discovery medicine*, 19(105):303, 2015.

J. B. Swann and M. J. Smyth. Immune surveillance of tumors. *The Journal of Clinical Investigation*, 117(5):1137–1146, 5 2007. doi: 10.1172/JCI31405. URL `https://www.jci.org/articles/view/31405`.

E. M. E. Verdegaal, N. F. C. C. de Miranda, M. Visser, T. Harryvan, M. M. van Buuren, R. S. Andersen, S. R. Hadrup, C. E. van der Minne, R. Schotte, H. Spits, J. B. A. G. Haanen, E. H. W. Kapiteijn, T. N. Schumacher, and S. H. van der Burg. Neoantigen landscape dynamics during human melanoma–t cell interactions. *Nature*, 536(7614):91–95, 2016. doi: 10.1038/nature18945. URL `https://doi.org/10.1038/nature18945`.

T.-C. Wang, M.-Y. Liu, J.-Y. Zhu, A. Tao, J. Kautz, and B. Catanzaro. High-resolution image synthesis and semantic manipulation with conditional gans. In *Proceedings of the IEEE Conference on Computer Vision and Pattern Recognition*, 2018.

S.-R. Woo, M. E. Turnis, M. V. Goldberg, J. Bankoti, M. Selby, C. J. Nirschl, M. L. Bettini, D. M. Gravano, P. Vogel, C. L. Liu, S. Tangsombatvisit, J. F. Grosso, G. Netto, M. P. Smeltzer, A. Chaux, P. J. Utz, C. J. Workman, D. M. Pardoll, A. J. Korman, C. G. Drake, and D. A. Vignali. Immune inhibitory molecules lag-3 and pd-1 synergistically regulate t-cell function to promote tumoral immune escape. *Cancer Research*, 72(4):917–927, 2012. ISSN 0008-5472. doi: 10.1158/0008-5472.CAN-11-1620. URL `https://cancerres.aacrjournals.org/content/72/4/917`.

T. Zhao and R. F. Murphy. Automated learning of generative models for subcellular location: Building blocks for systems biology. *Cytometry Part A*, 71A(12):978–990, 2007. doi: 10.1002/cyto.a.20487. URL `https://onlinelibrary.wiley.com/doi/abs/10.1002/cyto.a.20487`.

J.-Y. Zhu, T. Park, P. Isola, and A. A. Efros. Unpaired image-to-image translation using cycle-consistent adversarial networks. In *Computer Vision (ICCV), 2017 IEEE International Conference on*, 2017.